

Benchmarking five global optimization approaches for nano-optical shape optimization and parameter reconstruction

Philipp-Immanuel Schneider^{1,*}, Xavier Garcia Santiago^{1,2}, Victor Soltwisch³,
Martin Hammerschmidt¹, Sven Burger^{1,4}, and Carsten Rockstuhl^{2,5}

¹JCMwave GmbH, Bolivarallee 22, D-14 050 Berlin, Germany

²Institut für Nanotechnology, Karlsruher Institut für Technologie, PO-Box 3640, D-76 021
Karlsruhe, Germany

³Physikalisch-Technische Bundesanstalt (PTB), Abbestraße 2-12, D-10 587 Berlin, Germany

⁴Zuse Institute Berlin (ZIB), Takustraße 7, D-14 195 Berlin, Germany

⁵Institut für Theoretische Festkörperphysik, Karlsruher Institut für Technologie,
Wolfgang-Gaede-Str. 1, D-76 131 Karlsruhe, Germany

*Corresponding author: philipp.schneider@jcmwave.com

November 1, 2021

Abstract

Numerical optimization is an important tool in the field of computational physics in general and in nano-optics in specific. It has attracted attention with the increase in complexity of structures that can be realized with nowadays nano-fabrication technologies for which a rational design is no longer feasible. Also, numerical resources are available to enable the computational photonic material design and to identify structures that meet predefined optical properties for specific applications. However, the optimization objective function is in general non-convex and its computation remains resource demanding such that the right choice for the optimization method is crucial to obtain excellent results. Here, we benchmark five global optimization methods for three typical nano-optical optimization problems from the field of shape optimization and parameter reconstruction: downhill simplex optimization, the limited-memory Broyden-Fletcher-Goldfarb-Shanno (LBFGS) algorithm, particle swarm optimization, differential evolution, and Bayesian optimization. In these examples, Bayesian optimization, mainly known from machine learning applications, obtains significantly better results in a fraction of the run times of the other optimization methods.

1 Introduction

Numerical optimization is a fundamental task for many scientific and industrial applications. It is also an important tool in the field of nano-optics. Modern nano-

processing technologies such as laser writing [1] or 3D in-situ electron-beam lithography [2, 3] enable the fabrication of micro- and nano-optical structures with an increasing degree of accuracy and flexibility. From an experimental and technological perspective it is often not clear, which geometries and geometrical parameters lead to optimal results in terms of a desired functionality. Numerical simulation and scans of selected parameters can give important insights [4–7]. However, the full exploitation of the fabrication flexibility requires the simultaneous numerical optimization of all degrees of freedom. This process can be very time consuming and prompts for large computing resources (e. g. multi-core computers or computer clusters), fast simulation methods, and efficient numerical optimization methods that require as few as possible simulation results [8].

Another important application for numerical optimization is the parameter reconstruction based on measured data [9]. For example, optical scatterometry is the state-of-the-art optical inspection technique for quality control in lithographic processing [10]. This indirect measurement procedure relies on a parametrization of the specimen’s geometry and a numerical simulation of the measurement process. Based on multiple numerical simulations, one tries to identify the parameters that match best the measured data. Especially, for in-line quality control it is crucial to find the parameters with as few simulation runs as possible.

In each optimization scenario the first step is to define an objective function that maps the system’s parameters to an objective value that is to be minimized. In nano-optics the computation of the objective function gener-

ally requires to solve Maxwell’s equations. This can be achieved by different numerical methods depending on the geometry, such as the Finite-Element Method (FEM), rigorous coupled wave analysis (RCWA), and Finite-Difference Time-Domain (FDTD). In this work we use the software package JCMsuite [11], which employs the FEM approach in the frequency domain [12]. Typical computation times range from a few seconds for simple and highly symmetric systems to hours or even days for complex three-dimensional geometries with a spatial extent larger than many wavelengths. Nano-optical systems are often characterized by interference and resonance phenomena. Typically, by varying the dimensions of the system or the wavelength of the light, multiple resonances can be observed. As a consequence, the objective function is in general multi-modal. The existence of multiple minima makes it difficult to find the global minimum of the objective function. This is, for example, in contrast to the optimization problem of training artificial neural networks, where local minima seem not to be an obstacle in finding optimal network weights [13].

Optimization problems can be roughly divided into three groups: (1) low-dimensional problems (1 to 3 parameters), (2) medium-dimensional problems (4 to ~ 15 parameters) and (3) high-dimensional problems (~ 15 parameters to some hundred parameters or more). While low-dimensional problems often allow for scanning the full parameter space, this is already impossible for medium-dimensional problems. E.g., a scan of a 10-dimensional parameter space with a resolution of 100 different values for each parameter requires $100^{10} = 10^{20}$ evaluations of the objective function, rendering a regular parameter scan infeasible. This problem, known as *curse of dimensionality*, is tackled by global optimization approaches, which try to sample the parameter space in an effective way by avoiding regions with large function values. For high-dimensional problems, as they appear for example in the context of topology optimization, a global optimization is often impossible due to the exponentially growing number of possible parameter values to test. In this case, one often resorts to a local optimization method that explores the parameter space close to a given initial parameter vector [14] or one considers a discretization of the parameter space and applies evolutionary optimization techniques [15]. Alternatively, one can recast the optimization problem and solve for the Maxwell equations and the optimal material distribution simultaneously [16, 17].

In this work, we focus on medium-dimensional optimization problems that allow for a global optimization based on the solution of Maxwell’s equations, but do not allow for a complete scan of the parameter space. We consider two shape-optimization problems, i.e. the optimization of a single-photon source and the optimization of a dielectric metasurface. Further, we consider the problem of a geometrical parameter reconstruction based on X-ray diffraction measurements.

We benchmark optimization algorithms that can be broadly assigned to three categories: local optimization, global stochastic optimization and global model-based optimization.

- Starting from a given initial parameter vector, **local optimization methods** try to find better positions in the parameter space by exploring the neighborhood of the current position. They converge efficiently into a local minimum, which is not necessarily the global minimum. Gradient-based methods use first derivatives (gradients) or second derivatives (Hessians) in order to find a minimum in a smaller number of iterations. An example for a gradient-free method is the downhill simplex algorithm (also known as Nelder-Mead method) [18] and examples for gradient-based methods are the Broyden-Fletcher-Goldfarb-Shanno (BFGS) algorithm and its low-memory, bound-constrained extension L-BFGS-B [and references therein 19]. The gradient of the solution to Maxwell’s equations can be obtained by the adjointed method [20] or by automatic differentiation [21]. Local optimization methods have been used, e.g., to optimize a Y-junction splitter [20] or a photonic nano-antenna [22], and to reconstruct geometrical parameters of a line grating from scatterometry data [21].
- **Stochastic optimization algorithms** are based on random variables. Important representatives are particle swarm optimization [23] and differential evolution [24]. These algorithms usually scale well for an increasing number of dimensions. However, they tend to require many function evaluations in order to converge to the global minimum. Particle-swarm optimization has been employed for optimizing diffraction grating filters [25], photonic-crystal waveguides [26], or the duality symmetry of core-shell particles [27]. Differential evolution strategies have been lately investigated in the context of light focussing photonic crystals [28] and for parameter extraction of optical materials [29].
- **Model-based optimization methods** construct a model of the objective function in order to find promising sampling parameters. One important representative is Bayesian optimization, which constructs a statistical model of the objective function [30]. Bayesian optimization has a significant computation overhead on its own. Depending on the problem specification (number of parameters, number of acquired samples) the computation of the next sampling suggestion can take some seconds or even some minutes. Therefore, it is important to assess if this computational overhead is compensated by finding better parameter values in a lower number of iterations. This is one goal of this work. Bayesian optimization is regularly used in machine learning applications [30–32]. In the field

of nano-optics it has been employed to optimize ring resonator-based optical filters [33] and chiral scatterers [34].

Another machine-learning technique that has been recently applied for nano-optical optimization is deep learning [35]. Trained with thousands of simulation results deep neural networks can serve as accurate models for mapping a geometry to an optical response and vice versa almost instantaneously. However for this benchmark we only consider methods that do not require a training phase prior to the actual optimization.

The paper is organized as follows: In section 2 the considered optimization methods are introduced and strategies for their parallelization and support of parameter constraints are described. The three optimization problems are introduced in section 3. After the presentation and discussion of the numerical experiments in section 4 the paper concludes in section 5.

2 Examined optimization methods

In the field of optical simulations one has often access to computing clusters or powerful multi-core computers. It is therefore important that optimization methods exploit the possibility of computing the objective function for several input values in parallel. Moreover, it should be possible to distribute the computation of the objective function to several machines or threads. To this end, we have integrated the considered optimization methods in a server-client framework following the design strategy of Google Vizier [31]. Furthermore, we adapted the optimization methods to support inequality constraints of the parameter space that arise from geometrical or practical (e.g. fabrication) requirements. That is, one may provide a function $f_{\text{cons}} : \mathbf{x} \in \mathcal{X} \rightarrow \mathbb{R}$ for each constraint, such that only parameters \mathbf{x} with $f_{\text{cons}}(\mathbf{x}) \leq 0$ are sampled.

In the following, we shortly describe the approaches to support a parallel and constrained optimization for the considered optimization methods. Further details on the numerical framework, the implementation of the algorithms, and a visualization of the different optimization strategies are contained in Appendix A and B.

2.1 Local optimization methods

For local optimization methods, the next sampling point depends on the function value of the previous sample. A parallelization of local optimization methods is achieved by starting several independent local optimizations from different pseudo-random points in the parameter space $\mathcal{X} \subset \mathbb{R}^D$. For optimization problems that do not exploit derivative information, we consider the downhill simplex algorithm [18]. Otherwise, we consider the gradient-based L-BFGS-B algorithm [19]. Both

methods are implemented based on the python package `scipy.optimize` [36].

If the optimization methods compute a sampling point \mathbf{x} that does not meet a constraint, i.e. $f_{\text{cons}}(\mathbf{x}) > 0$, the sampling point is not sent to the client for evaluation. Instead, the optimization method is provided with the function value $f_{\text{max}} + f_{\text{cons}}(\mathbf{x})$ and the gradient $\nabla f_{\text{cons}}(\mathbf{x})$, where f_{max} is the maximal function value seen so far. This procedure is repeated until the optimization method computes a sampling point that meets the constraints.

2.2 Stochastic global optimization

As stochastic global optimization methods, we consider particle swarm optimization and differential evolution.

Particle swarm optimization works by randomly moving the position of each particle in the search-space guided by the particle’s best known position as well as the swarm’s best known position. The method is implemented based on the Python package `pyswarm` [37], which supports a parallel evaluation of the objective function. As an extension, the random update of the particle positions is repeated until all constraints are met. If this fails 100 times, the particle is randomly placed somewhere else in the constrained parameter space $\mathcal{X} \subset \mathbb{R}^D$.

Differential evolution is a population-based genetic algorithm that is implemented based on the python package `scipy.optimize.differential_evolution` [36, 38]. We extend the algorithm by repeating the crossover until new offsprings fulfill the constraints. Furthermore, we allow for a parallel evaluation of the fitness function for each offspring.

2.3 Bayesian optimization

Bayesian optimization is based on a stochastic model of the objective function. We employ a Gaussian process (GP) that is updated with each new evaluation of the objective function [30]. The parallelization is realized as proposed by González *et al.* [39] (see Appendix A for details).

The GP allows to identify parameter values with a large expected improvement $\text{EI}(\mathbf{x})$. The search process for the next sampling point

$$\mathbf{x}^* = \arg \max_{\mathbf{x} \in \mathcal{X}} [\text{EI}(\mathbf{x})]$$

is itself an optimization problem that can be computationally demanding. Usually, the evaluation of the objective function, which requires to solve Maxwell’s equations, is much more time consuming than an evaluation of the GP. However, the evaluation time of the GP grows at least quadratically with the number of observations. It is, therefore, important to balance the effort to find \mathbf{x}^* with the effort to compute the objective function.

The search for \mathbf{x}^* is performed with the L-BFGS-B method starting from a number N_{init} of different initial

points. If a sampling point \mathbf{x} computed by the L-BFGS-B optimization does not meet a constraint (i.e. $f_{\text{cons}}(\mathbf{x}) > 0$), the function value $f_{\text{cons}}(\mathbf{x})$ and the gradient $\nabla f_{\text{cons}}(\mathbf{x})$ are returned to the L-BFGS-B optimizer. To reduce the computational time of the search, we adapt at each iteration the number of starting points N_{init} and the maximum number of evaluations of the GP N_{GP} of each L-BFGS-B run. This is done with the aim to limit the search time t_s to the computation time of the objective function t_{obj} divided by the desired number of parallel evaluations of the objective function. In order to achieve a speedup S of the search time t_s , we divide N_{init} and N_{GP} by \sqrt{S} .

One important advantage of Bayesian optimization is, that GP regression does not rely on derivative information on the objective function, but that one can incorporate derivative information if they are available [40]. As will be shown in Sec. 4 this can speed up the optimization significantly.

3 Optimization Problems

For benchmarking the different optimization algorithms, we consider three technologically relevant optimization problems of contemporary interest: the maximization of the coupling efficiency of a single-photon source to an optical fiber, the parameter reconstruction of a lamellar grating from scattering data, and the reflection suppression from a silicon metasurface.

3.1 Improving the coupling efficiency of a single-photon source

Single-photon sources are essential building blocks of future photonic and quantum optical devices. We consider a source consisting of a quantum dot (QD) emitting at a vacuum wavelength of $\lambda = 1,300$ nm in the telecom O-band. The QD is embedded into a mesa structure made from gallium arsenide (GaAs; refractive index $n_{\text{GaAs}} = 3.4$). An underlying Bragg reflector made from layers of GaAs and aluminum gallium arsenide ($\text{Al}_{0.9}\text{Ga}_{0.1}\text{As}$; $n_{\text{AlGaAs}} = 3.0$) reflects the light emitted by the QD back into the upper hemisphere. The light is coupled into an optical fiber with large numerical aperture (NA) above the QD consisting of a homogeneous fiber core and a homogeneous fiber cladding ($n_{\text{core}} = 1.5$, $n_{\text{clad}} = 1.45$, $\text{NA} \equiv \sqrt{n_{\text{core}}^2 - n_{\text{clad}}^2} = 0.38$). The setup is sketched in Fig. 1 a).

The parameter space \mathcal{X} is spanned by 6 parameters, the height of the top layer above the Bragg reflector (h_{layer}), the diameter of the fiber core (d_{core}), the width and height of the mesa (w_{mesa} , h_{mesa}), the elevation of the dipole within the mesa (h_{dip}), and the distance between mesa and fiber (s_{mf}). The objective of the optimization is to maximize the coupling efficiency of the emitted light into the fundamental modes of the fiber. The numerical

method to determine the coupling efficiency is described in [41].

3.2 Parameter reconstruction of a lamellar grating

Grazing incidence small angle X-ray scattering (GISAXS) is a destruction-free scatterometry method. With incidence angles close to the critical angle of total external reflection, GISAXS is a technique with high surface sensitivity. We consider the parameter reconstruction of a periodic, lamellar silicon grating manufactured by electron beam lithography [42]. The grating geometry is modeled by 5 parameters, the critical dimension CD (line width), the line height h_{line} , the side-wall angle ϕ_{swa} , the top corner radius r_{top} , and the depth of the grooves d_{groove} [see Fig. 2 a)]. A monochromatic X-ray beam idealized as a plane wave with the wave vector \mathbf{k}_{in} impinges on the sample surface at a grazing incidence angle. The elastically scattered wave with the wave vector \mathbf{k}_{f} propagates to a 2D area detector that records a scattering intensity pattern $I_{\text{det}}(\mathbf{q})$ as a function of the scattering vector $\mathbf{q} = \mathbf{k}_{\text{f}} - \mathbf{k}_{\text{in}}$ [see Fig. 2 b)]. Based on a FEM model of the experiment, one can determine a scattering intensity $I_{\text{FEM}}(\mathbf{p}, \alpha_{\text{in}}, \theta_{\text{im}}, E, N)$ for each parameter set $\mathbf{p} \in \mathcal{X}$, photon energy E , and diffraction order N [42].

The natural line edge and line width roughness of the grating is taken into account with an analytic approach based on Debye-Waller damping $\exp(-[\sigma_{\text{r}}\mathbf{q}_y(N)]^2)$ with the damping factor σ_{r} and the y -component $\mathbf{q}_y(N)$ of the scattering vector for diffraction order N . Furthermore, the model intensities are scaled by an energy-dependent factor $s(E)$ in order to account for the unknown effective illumination area of the sample.

This leads to the following model for the measured intensities in each diffraction order N

$$I_{\text{model}}(\mathbf{p}, E, N) = I_{\text{FEM}}(\mathbf{p}, E, N) s(E) \exp(-[\sigma_{\text{r}}\mathbf{q}_y(N)]^2).$$

The data acquisition is performed for three different photon energies, $E_1 = 5.5$ keV, $E_2 = 5.55$ keV, and $E_3 = 5.6$ keV. For each energy, the standard deviation $\sigma(E_i)$ of the measured intensities was determined, as described in [42]. The aim of the optimization is to minimize the mean squared numerical error of all diffraction orders and energies

$$\chi^2 = \sum_{i=1}^3 \sum_{N=1}^M \frac{(I_{\text{model}}(\mathbf{p}, E_i, N) - I_{\text{exp}}(E_i, N))^2}{\sigma^2(E_i)} \quad (1)$$

with respect to the geometrical parameters CD, h_{line} , ϕ_{swa} , r_{top} , d_{groove} , the roughness σ_{r} , and the three scaling factors $s_i = s(E_i)$ for $i = 1, 2, 3$.

We note, that it is straightforward to determine the derivatives of χ^2 with respect to the parameters σ_{r} , s_1 , s_2 , and s_3 that do not enter into the numerical FEM simulation of the measurement process. In Sec. 4 we will make use of these derivative information in order to assess to

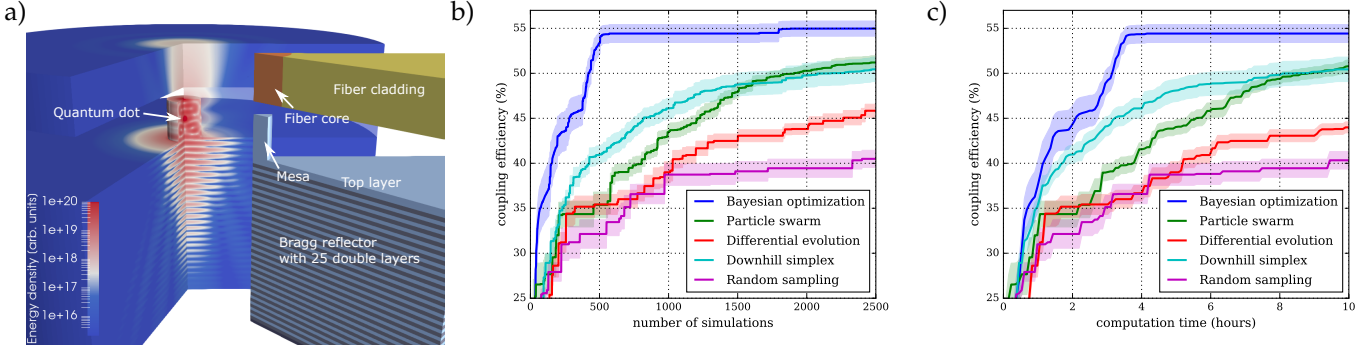


Fig. 1. **a)** Visualization of the energy density of the light field of the optimized fiber-coupled single-photon source with a coupling efficiency of 60%. A cut through the geometry is shown in front of the energy-density plot. The single-photon source consists of a QD dipole source embedded into a mesa structure (GaAs, blue), a Bragg reflector (alternating layers of GaAs (blue) and $\text{Al}_{0.9}\text{Ga}_{0.1}\text{As}$ (gray)), and an optical fiber with homogeneous fiber core (orange) and fiber cladding (yellow). The Bragg reflector is grown on a substrate made of GaAs and has a GaAs top layer (blue). The six optimized parameters are the mesa height $h_{\text{mesa}} = 1217$ nm, mesa width $w_{\text{mesa}} = 1044$ nm, top-layer thickness $h_{\text{layer}} = 190$ nm, dipole elevation within the mesa $h_{\text{dip}} = 613$ nm, fiber-core diameter $d_{\text{core}} = 1937$ nm, and mesa-fiber distance $s_{\text{mf}} = 352$ nm. **b):** Best seen coupling efficiency for different optimization approaches as a function of the number of simulations averaged over six independent optimization runs. The shading indicates the uncertainty of the average. **c):** Same as b) but the best seen coupling efficiency is shown as a function of the total computation time. The comparison with a) shows that Bayesian optimization has a significant computational overhead for calculating the next sampling point. Nevertheless, it outperforms the other optimization approaches.

which extend partial information on parameter derivatives can speed up the Bayesian optimization process.

3.3 Reflection suppression of a metasurface

Broadband antireflection is a desirable property, e.g., for high-efficiency solar cells as well as for CCD or CMOS sensors. We consider a nano-structured silicon metasurface for suppressing the reflectivity in a broad range of frequencies [43]. The metasurface consists of a square array of silicon bumps on top of a silicon substrate [see Fig. 2 a)] and is parametrized by six length scales: the periodicity of the array (p), the heights of the lower and upper part of the bumps ($h_{\text{lower}}, h_{\text{upper}}$), and the bottom, middle and top width of the bumps ($w_{\text{bottom}}, w_{\text{middle}}, w_{\text{top}}$). The reflectivity of incident plane waves perpendicular to the surface is averaged over four wavelengths, 500 nm, 600 nm, 700 nm, and 800 nm. In order to facilitate the fabrication of the structure we constrain the parameter space of the optimization such that $w_{\text{bottom}} \leq p - 10$ nm, $w_{\text{bottom}} \leq w_{\text{middle}} \leq w_{\text{top}}$ and $h_{\text{lower}} + h_{\text{upper}} \leq 2w_{\text{bottom}}$.

Based on automatic differentiation, the FEM software JCMSuite [11] allows to determine partial derivatives of the computed fields with respect to geometrical parameters with small computational overhead. Based on this information, we compute for this example the partial derivatives of the reflectivity with respect to the six design parameters.

4 Numerical experiments

The optimization runs for the three optimization problems introduced in the previous section have been each performed for a fixed number of iterations (single-photon source optimization and parameter reconstruction 2,500 iterations, antireflective metasurface optimization 500 iterations). In order to evaluate the average performance of the different optimization methods, each run has been repeated 6 times with different initial conditions.

In addition to the optimization methods introduced in Sec. 2, results for a random sampling of the objective functions are also considered. Random sampling is a non-informative method and thus presents a baseline approach. If an optimization method is not significantly better than random sampling, it suffers from the specific properties of the objective function, e.g. irregularities or the existence of too many local minima.

The optimization of the single-photon source and the parameter reconstruction were performed on a machine with a 6-core Intel Xeon CPUs running at 3.2 GHz with 11 GB of RAM. The optimization methods were configured to perform at most 4 parallel computations of the objective function. The optimization of the metasurface is numerically much more demanding as a three-dimensional geometry is considered and a wavelength scan has to be performed. Therefore, the optimizations were run on a more powerful machine with 4 Intel Xeon CPUs with 10 cores at 2.4 GHz with 1 TB of RAM. Up to 6 parallel computations of the objective function were performed.

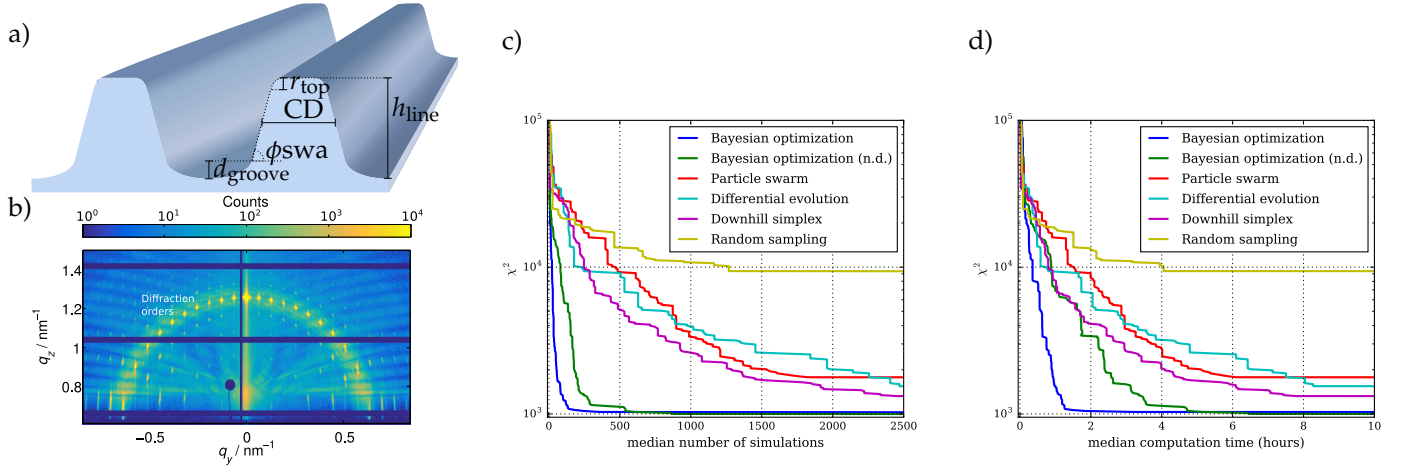


Fig. 2. **a)** Geometry of the lamellar grating. The aim of the GISAXS measurement is to reconstruct the critical dimension CD, the line height h_{line} , the side-wall angle ϕ_{swa} , the top corner radius r_{top} , and the depth of the grooves d_{groove} . **b)** GISAXS scattering pattern of the grating obtained at a photon energy of 6.5 keV shown as a function of the scattering vector components q_y and q_z . The intensity is shown with a logarithmic false color scale. **c):** Error χ^2 [see Eq. (1)] for different optimization approaches as a function of the median number of simulations needed to reach a value below χ^2 for six independent optimization runs. The blue and green lines show the results of Bayesian optimization including derivatives and using no derivative (n.d.) information, respectively. **d):** Same as c) but χ^2 is shown as a function of the median total computation time.

4.1 Optimized single-photon source

Figure 1 b) and c) compares the performance of Bayesian optimization, particle swarm optimization, differential evolution, the downhill simplex method, and random sampling for the example of the maximization of the coupling efficiency of the emitted light into the optical fiber. Bayesian optimization clearly outperforms all other methods. After only 500 iterations and a computation time of 3.5 hours it reaches an average coupling efficiency of 54% while the other optimization methods reach only average efficiencies below 52% after 2,500 iteration and a computation time of 10 hours.

A comparison of Fig. 1 b) and c) shows that Bayesian optimization has a significant computational overhead compared to the other optimization approaches, which can determine the next sampling point on a negligible time scale. For Bayesian optimization the calculation of the next sampling point took on average 21 seconds while the simulations itself took 58 seconds. Despite this significant overhead, the sampling strategy of Bayesian optimization leads to much smaller total computation times.

The computed optimal configuration with mesa height $h_{\text{mesa}} = 1217$ nm, mesa width $w_{\text{mesa}} = 1044$ nm, top-layer thickness $h_{\text{layer}} = 190$ nm, dipole elevation $h_{\text{dip}} = 613$ nm, fiber-core diameter $d_{\text{core}} = 1937$ nm, and mesa-fiber distance $s_{\text{mf}} = 352$ nm is shown in Fig. 1 a). The setup achieves a remarkably large coupling efficiency of 60% to the optical fiber. In a previous work, we tried to improve the coupling efficiency of the same system by performing numerical scans of all parameters of the geometry apart from the top-layer thickness h_{layer} ,

which was fixed to 195 nm. A full parameter scan of all five parameters with only 10 values per parameter would have required 100,000 simulations. Therefore, we restricted the scan to a small fraction of the physically realizable parameter space. For example, we restricted the parameter scan of the dipole elevation to values between 0 and 50 nm in steps of 10 nm, while for the current optimization we considered values between 0 and 1000 nm. Due to this restriction a maximal coupling efficiency of only 23% was obtained [41]. This demonstrates that an optimization within a large space of realizable system parameters is important to assess the technological potential of a nano-optical system.

4.2 Parameter reconstruction

For practical applications of shape optimization it is of interest to determine a reasonably good structure in a limited time budget (e.g. in one day). In contrast, in the context of a parameter reconstruction it is important to find parameter values close to the *global* optimum with a small error level χ^2 as fast as possible. Correspondingly, Fig. 2 c) and d) shows the *median* number of simulations and the *median* time span needed to reach a specific error level χ^2 . The optimal parameters correspond to the values obtained already in Ref. [42].

In this case, Bayesian optimization shows an impressive lead in comparison with the other optimization methods. Using the derivative information with respect to the parameters σ_r, s_1, s_2, s_3 Bayesian optimization reaches the global minimum after a medium number of about 250 simulations and a medium time of less than

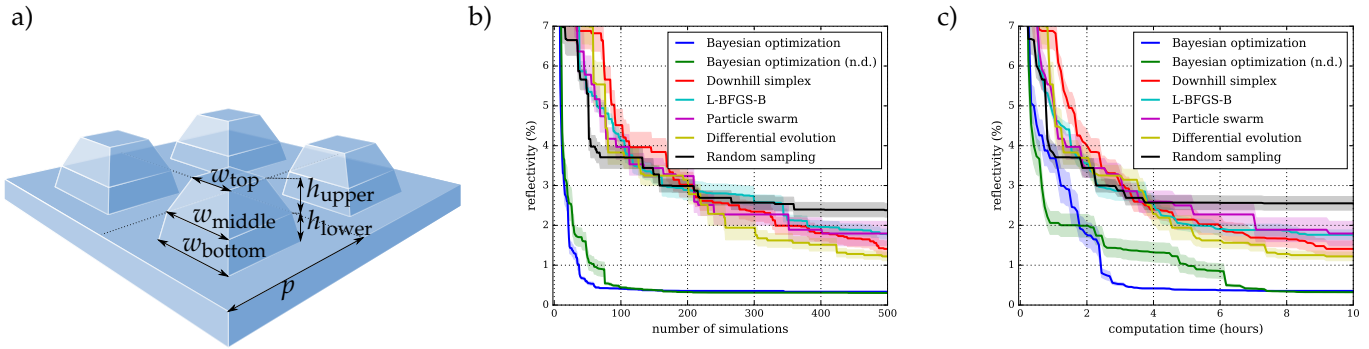


Fig. 3. a): The metasurface consists of a square array of silicon bumps on a silicon substrate. The reflectivity of the structure is minimized with respect to the periodicity of the array (p), the heights of the lower and upper part of the bumps (h_{lower} and h_{upper}), and the bottom, middle and top width of the bumps (w_{bottom} , w_{middle} and w_{top}). **b):** Lowest reflectivity for different optimization approaches as a function of the number of simulations averaged over six independent optimization runs. The shading indicates the uncertainty of the average. **c):** Same as b) but the lowest reflectivity is shown as a function of the total computation time. Bayesian optimization using no derivative information ["Bayesian optimization (n.d.)"] takes roughly twice as long to obtain a reflectivity below 0.5%. Other optimization approaches reach only significantly higher reflectivity values.

two hours (blue line), while the non-Bayesian methods do not manage to find the global minimum even after 2,500 iterations or eight hours computation time.

4.3 Optimized antireflective metasurface

For the example of the reflection suppression of the metasurface, all first order partial derivatives with respect to the six geometrical parameters were determined by automatic differentiation. This enables to apply also the gradient-based L-BFGS-B method. The benchmark results are presented in Fig. 3 b) and c). Again Bayesian optimization, even without using derivative information ("Bayesian optimization (n.d.)"), optimizes the structure significantly faster and it is the only optimization method that reaches average reflectivities below 0.5% while other optimization methods reach average reflectivities between 1% and 2%. The use of derivatives for Bayesian optimization offers again a significant advantage. It is remarkable that this is not the case for L-BFGS-B optimization, which performs comparable to the other non-derivative methods, including random sampling. We attribute this to a complex shape of the objective function with many similarly low local minima.

For the shape optimization the reflectivity of the metasurface was averaged over only four wavelength values (500 nm, 600 nm, 700 nm, and 800 nm) in order to reduce the computational time for evaluating the objective function. Still, for this three dimensional problem, the average computation times was with five minutes significantly larger than for the two other optimization problems. Correspondingly, the Bayesian optimization approach could spend more time (in average two minutes) to compute new samples while other objective values were computed.

The best geometry with the parameter values $h_{\text{lower}} = 227.6$ nm, $h_{\text{upper}} = 236.7$ nm, $w_{\text{bottom}} = 236.4$ nm, $w_{\text{middle}} = 222.6$ nm, $w_{\text{top}} = 66.4$ nm, and $p = 237.4$ nm has an objective value of 0.28% reflectivity. In Fig. 4, the optimal geometry is shown together with a full wavelength scan of its reflectivity in the range of 400 nm to 900 nm. As expected, the reflectivity outside the optimization range of 500 nm to 800 nm increases significantly. Still, the average reflectivity in the range of 400 nm to 900 nm is only 0.87%.

In comparison with previous numerical studies on silicon metasurfaces, much lower reflectivities could be obtained. For example, in [43] a minimal averaged reflectivity of 4% was reached in the range of 400 nm to 900 nm. In [43] the optimization was performed with the help of parameter scans within a three-dimensional parameter space (periodicity of square array, width and height of silicon bumps). This again demonstrates, that an optimization within a larger parameter space can significantly improve the performance of nano-optical structures with respect to parameter scans in a small subspace.

5 Conclusion

We compared five state-of-the-art optimization methods and applied them to three characteristic nano-optical optimization problems: the maximization of the coupling efficiency of a single-photon source, the reconstruction of geometrical parameters based on scatterometry data, and the suppression of the reflectivity of a silicon metasurface. The optimization methods were extended to meet typical requirements of computational nano-optics, i.e. the parameter space can be constrained by inequalities and several objective function values can be computed in parallel. All methods were run with typical numerical

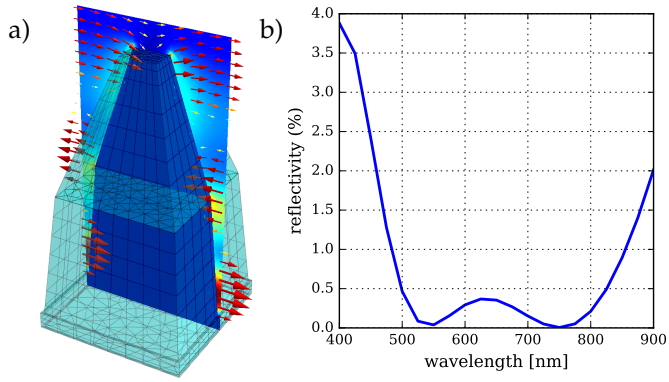


Fig. 4. a): Optimal geometry of a single bump of the square lattice with $h_{\text{lower}} = 227.6$ nm, $h_{\text{upper}} = 236.7$ nm, $w_{\text{bottom}} = 236.4$ nm, $w_{\text{middle}} = 222.6$ nm, $w_{\text{top}} = 66.4$ nm, and $p = 237.4$ nm. Note that the periodicity p is only 10 nm larger than the bottom width w_{bottom} of the bumps. Furthermore, the electric field is visualized by an intensity profile and electric field vectors evincing large field intensity in the gaps between the bumps. **b):** Wavelength scan of the reflectivity for the optimized structure. The metasurface has an average reflectivity 0.2% in the wavelength range of 500 nm to 800 nm and 0.87% in the range of 400 nm to 900 nm.

setting, i.e. without a manual targeted adaptation to the optimization problems.

The numerical experiments showed that Bayesian optimization runs significantly faster than the other considered methods, downhill simplex optimization, L-BFGS-B, particle swarm optimization, and differential evolution. That is, Bayesian optimization reaches good objective function values in only a fraction of the computation times of the other methods, although it has a larger computational overhead. The use of derivative information with respect to some or all parameters can further reduce the run times of Bayesian optimization.

The properties of the optimized single-photon source and the antireflective metasurface are considerably better than those obtained previously from parameter scans. The results suggest that, whenever possible, one should perform global optimizations within the physically feasible parameter space in order to assess the technological potential of a nano-optical structure.

Funding Information

This project has received funding from the European Unions Horizon 2020 research and innovation programme under the Marie Skłodowska-Curie grant agreement No 675745 (MSCA-ITN-EID NOLOSS). Further, we acknowledge financial support from the EMPIR programme co-financed by the Participating States and from the European Union's Horizon 2020 research and in-

novation programme under grant agreement number 17FUN01 (BeCOME). We also acknowledge support by KIT through the Virtual Materials Design (VIRT-MAT) project by the Helmholtz Association via the Helmholtz program Science and Technology of Nanosystems (STN).

References

1. J. Fischer and M. Wegener, "Three-dimensional optical laser lithography beyond the diffraction limit," *Laser Photonics Rev.* **7**, 22–44 (2011).
2. G. Yoon, I. Kim, S. So, J. Mun, M. Kim, and J. Rho, "Fabrication of three-dimensional suspended, interlayered and hierarchical nanostructures by accuracy-improved electron beam lithography overlay," *Sci. reports* **7**, 6668 (2017).
3. A. Kaganskiy, S. Fischbach, A. Strittmatter, S. Rodt, T. Heindel, and S. Reitzenstein, "Enhancing the photon-extraction efficiency of site-controlled quantum dots by deterministically fabricated microlenses," *Opt. Commun.* **413**, 162 – 166 (2018).
4. M. Gschrey, A. Thoma, P. Schnauber, M. Seifried, R. Schmidt, B. Wohlfeil, L. Krüger, J.-H. Schulze, T. Heindel, S. Burger, F. Schmidt, A. Strittmatter, S. Rodt, and S. Reitzenstein, "Highly indistinguishable photons from deterministic quantum-dot microlenses utilizing three-dimensional in situ electron-beam lithography," *Nat. Commun.* **6**, 7662 (2015).
5. Y. Chen, T. R. Nielsen, N. Gregersen, P. Lodahl, and J. Mørk, "Finite-element modeling of spontaneous emission of a quantum emitter at nanoscale proximity to plasmonic waveguides," *Phys. Rev. B* **81**, 125431 (2010).
6. G. Bulgarini, M. E. Reimer, M. Bouwes Bavinck, K. D. Jöns, D. Dalacu, P. J. Poole, E. P. A. M. Bakkers, and V. Zwiller, "Nanowire waveguides launching single photons in a gaussian mode for ideal fiber coupling," *Nano Lett.* **14**, 4102–4106 (2014).
7. J. Yang, J.-P. Hugonin, and P. Lalanne, "Near-to-far field transformations for radiative and guided waves," *ACS Photonics* **3**, 395–402 (2016).
8. W. Bogaerts and L. Chrostowski, "Silicon photonics circuit design: Methods, tools and challenges," *Laser Photonics Rev.* **12**, 1700237 (2017).
9. L. Pang, D. Peng, P. Hu, D. Chen, L. He, Y. Li, M. Satake, and V. Tolani, "Computational metrology and inspection (CMI) in mask inspection, metrology, review, and repair," *Adv. Opt. Techn.* **1**, 299–321 (2012).
10. B. Bodermann, G. Ehret, J. Endres, and M. Wurm, "Optical dimensional metrology at Physikalisch-Technische Bundesanstalt (PTB) on deep sub-wavelength nanostructured surfaces," *Surf. Topogr.* **4**, 024014 (2016).

11. "JCMsuite - software solutions for nanooptics," <https://jcmwave.com> (2018).
12. P. Monk, *Finite Element Methods for Maxwell's Equations* (Clarendon Press, 2003).
13. I. J. Goodfellow, O. Vinyals, and A. M. Saxe, "Qualitatively characterizing neural network optimization problems," arXiv preprint arXiv:1412.6544 (2014).
14. A. Y. Piggott, J. Petykiewicz, L. Su, and J. Vučković, "Fabrication-constrained nanophotonic inverse design," *Sci. Rep.* **7**, 1786 (2017).
15. J. Hu, X. Ren, A. N. Reed, T. Reese, D. Rhee, B. Howe, L. J. Lauhon, A. M. Urbas, and T. W. Odom, "Evolutionary design and prototyping of single crystalline titanium nitride lattice optics," *ACS Photonics* **4**, 606–612 (2017).
16. J. Lu and J. Vučković, "Nanophotonic computational design," *Opt. Express* **21**, 13351–13367 (2013).
17. A. Y. Piggott, J. Lu, K. G. Lagoudakis, J. Petykiewicz, T. M. Babinec, and J. Vučković, "Inverse design and demonstration of a compact and broadband on-chip wavelength demultiplexer," *Nat. Photonics* **9**, 374–377 (2015).
18. J. A. Nelder and R. Mead, "A simplex method for function minimization," *Comput. J.* **7**, 308–313 (1965).
19. R. H. Byrd, P. Lu, J. Nocedal, and C. Zhu, "A limited memory algorithm for bound constrained optimization," *SIAM J. Sci. Comput.* **16**, 1190–1208 (1995).
20. C. M. Lalau-Keraly, S. Bhargava, O. D. Miller, and E. Yablonovitch, "Adjoint shape optimization applied to electromagnetic design," *Opt. Express* **21**, 21693–21701 (2013).
21. M. Hammerschmidt, M. Weiser, X. G. Santiago, L. Zschiedrich, B. Bodermann, and S. Burger, "Quantifying parameter uncertainties in optical scatterometry using Bayesian inversion," *Proc. SPIE* **10330**, 1033004 (2017).
22. N. Nikolay, G. Kewes, and O. Benson, "A compact and simple photonic nano-antenna for efficient photon extraction from nitrogen vacancy centers in bulk diamond," arXiv preprint arXiv:1704.08951 (2017).
23. Y. Zhang, S. Wang, and G. Ji, "A comprehensive survey on particle swarm optimization algorithm and its applications," *Math. Probl. Eng.* **2015**, 931256 (2015).
24. S. Das and P. N. Suganthan, "Differential evolution: A survey of the state-of-the-art," *IEEE Trans. Evol. Comput.* **15**, 4–31 (2011).
25. M. Shokoh-Saremi and R. Magnusson, "Particle swarm optimization and its application to the design of diffraction grating filters," *Opt. Lett.* **32**, 894–896 (2007).
26. S. M. Mirjalili, K. Abedi, and S. Mirjalili, "Optical buffer performance enhancement using particle swarm optimization in ring-shape-hole photonic crystal waveguide," *Optik*. **124**, 5989 – 5993 (2013).
27. A. Rahimzadegan, C. Rockstuhl, and I. Fernandez-Corbaton, "Core-shell particles as building blocks for systems with high duality symmetry," *Phys. Rev. Appl.* **9**, 054051 (2018).
28. E. Bor, M. Turduev, and H. Kurt, "Differential evolution algorithm based photonic structure design: numerical and experimental verification of subwavelength $\lambda/5$ focusing of light," *Sci. Rep.* **6**, 30871 (2016).
29. M. G. Saber, A. Ahmed, and R. H. Sagor, "Performance analysis of a differential evolution algorithm in modeling parameter extraction of optical material," *Silicon*. **9**, 723–731 (2017).
30. B. Shahriari, K. Swersky, Z. Wang, R. P. Adams, and N. De Freitas, "Taking the human out of the loop: A review of Bayesian optimization," *Proc. IEEE* **104**, 148–175 (2016).
31. D. Golovin, B. Solnik, S. Moitra, G. Kochanski, J. Karro, and D. Sculley, "Google vizier: A service for black-box optimization," in *Proceedings of the 23rd ACM SIGKDD International Conference on Knowledge Discovery and Data Mining*, (ACM, New York, NY, USA, 2017), KDD '17, pp. 1487–1495.
32. "How hyperparameter tuning works on amazon sagemaker," <https://docs.aws.amazon.com/sagemaker/latest/dg/automatic-model-tuning-how-it-works.html> (2018).
33. S. U. Rehman and M. Langelaar, "System robust optimization of ring resonator-based optical filters," *J. Light. Technol.* **34**, 3653–3660 (2016).
34. P. Gutsche, P.-I. Schneider, S. Burger, and M. Nieto-Vesperinas, "Chiral scatterers designed by Bayesian optimization," *J. Phys. Conf. Ser.* **963**, 012004 (2018).
35. I. Malkiel, M. Mrejen, A. Nagler, U. Arieli, L. Wolf, and H. Suchowski, "Plasmonic nanostructure design and characterization via deep learning," *Light. Sci. & Appl.* **7**, 60 (2018).
36. E. Jones, T. Oliphant, P. Peterson *et al.*, "SciPy: Open source scientific tools for Python," (2001–).
37. A. Lee, "pyswarm: Particle swarm optimization (pso) with constraint support," <https://github.com/tisimst/pyswarm> (2014).
38. "Documentation on scipy.optimize.differential_evolution," https://docs.scipy.org/doc/scipy-0.17.0/reference/generated/scipy.optimize.differential_evolution.html (2016).
39. J. Gonzalez, Z. Dai, P. Hennig, and N. Lawrence, "Batch Bayesian optimization via local penalization," in *Proceedings of the 19th International Conference on Artificial Intelligence and Statistics*, , vol. 51 of *Proc. Mach. Learn. Res.* (2016), pp. 648–657.
40. E. Solak, R. Murray-Smith, W. E. Leithead, D. J. Leith, and C. E. Rasmussen, "Derivative observations in Gaussian process models of dynamic systems," in *Advances in neural information processing systems*, (2003), pp. 1057–1064.
41. P.-I. Schneider, N. Srocka, S. Rodt, L. Zschiedrich,

- S. Reitzenstein, and S. Burger, "Numerical optimization of the extraction efficiency of a quantum-dot based single-photon emitter into a single-mode fiber," *Opt. Express* **26**, 8479–8492 (2018).
42. V. Soltwisch, A. Fernández Herrero, M. Pflüger, A. Haase, J. Probst, C. Laubis, M. Krumrey, and F. Scholze, "Reconstructing detailed line profiles of lamellar gratings from GISAXS patterns with a Maxwell solver," *J. Appl. Crystallogr.* **50**, 1524–1532 (2017).
 43. J. Proust, A.-L. Fehrembach, F. Bedu, I. Ozerov, and N. Bonod, "Optimized 2d array of thin silicon pillars for efficient antireflective coatings in the visible spectrum," *Sci. Rep.* **6**, 24947 (2016).
 44. I. M. Sobol', "On the distribution of points in a cube and the approximate evaluation of integrals," *Zh. Vychisl. Mat. Mat. Fiz.* **7**, 784–802 (1967).
 45. C. Chisari, "Sobol: The sobol quasirandom sequence," http://people.sc.fsu.edu/~jburkardt/py_src/sobol/sobol.html (2014).
 46. A. Wu, M. C. Aoi, and J. W. Pillow, "Exploiting gradients and Hessians in Bayesian optimization and Bayesian quadrature," arXiv preprint arXiv:1704.00060 (2017).
 47. P.-I. Schneider, X. Garcia Santiago, C. Rockstuhl, and S. Burger, "Global optimization of complex optical structures using Bayesian optimization based on Gaussian processes," *Proc. SPIE* **10335**, 103350C (2017).
 48. X. Garcia-Santiago, P.-I. Schneider, C. Rockstuhl, and S. Burger, "Shape design of a reflecting surface using Bayesian optimization," *J. Phys. Conf. Ser.* **963**, 012003 (2018).

```

# Definition of the search domain
domain = [
    {'name': 'x1', 'domain': (-2,2)},
    {'name': 'x2', 'domain': (0,20)}
]

# Definition of constraints, here x1 < x2,
# i.e. x1 - x2 < 0
constraints = [
    {'name': 'constraint1', 'constraint': 'x1
    - x2'}
]

# Setup of the optimization study with 1000
# iterations and 4 parallel objective
# evaluations
study = client.create_study(domain, constraints
)
study.set_parameters(max_iter=1000,
    num_parallel=4)

# Optimization run
while not study.is_done():
    # Obtain a new suggestion from the server
    suggestion = study.get_suggestion()
    # Start a new thread to compute the
    # objective
    threading.Thread(target=acquire, args=(
        suggestion,)).start()

# thread-based parallel acquisition of the
# objective
def acquire(suggestion):
    # Compute the objective, e.g. on a cluster
    observation = ComputeObjective(**
        suggestion.kwargs)
    # Report back the observation to the
    # server
    study.add_observation(observation,
        suggestion.id)

```

The search domains of the three optimization problems described in the main text are summarized in Tab. 1.

Appendices

The appendices provide supplementary information regarding the implementation and numerical setting of the optimization methods as well as a visualization of the different optimization strategies.

A Implementation and setting of optimization methods

In the field of optical simulations one has often access to computing clusters or powerful multi-core computers. Many numerical frameworks such as the python package `scipy` enable only a sequential optimization. That is, only one objective function value is evaluated at a time. In order to allow for a parallel evaluation of the objective function and for a distribution of the computation of the objective function to several machines, we have integrated the considered optimization methods in a server-client framework. The following python code represents a small example for setting up a constrained optimization study on the client side:

A.1 Local optimization methods

For a parallelization of local optimization methods, several independent local optimization runs are started from different points in the parameter space $\mathcal{X} \subset \mathbb{R}^D$. To get a good coverage of the parameter space, we draw starting points from a pseudo-random Sobol sequence [44, 45]. After a local optimization has converged, it is restarted at a new point from the Sobol sequence. In all benchmark problems, the local optimization methods are started from 10 different initial points.

For optimization problems that do not exploit derivative information, we consider the downhill simplex algorithm [18]. For a D dimensional parameter space $\mathcal{X} \subset \mathbb{R}^D$, the simplices consist of $D + 1$ points $\mathbf{x}_0, \dots, \mathbf{x}_D$. In each step the point \mathbf{x}_h with the largest function value is replaced by a better one by testing candidates along the line connecting the central point of the simplex and \mathbf{x}_h . If this fails, the simplex is contracted and eventually converges to a local minimum. We initialize the simplices such that they span 10% of the search domain \mathcal{X} in each parameter dimension.

Table 1. Parameter ranges of the search domains for the three optimization problems. All length scales are given in nanometers, the angle ϕ_{swa} is given in degree, and the scaling factors s_i ($i = 1, 2, 3$) are without units. See the main text for the definition of the parameters.

Single-photon source							
	h_{layer}	d_{core}	w_{mesa}	h_{mesa}	h_{dip}	s_{mf}	
min.	10	1000	500	500	0	0	
max.	150	3000	1500	1500	1000	1000	
Parameter reconstruction							
	CD	h_{line}	ϕ_{swa}	r_{top}	d_{groove}	σ_{r}	s_i
min.	60	115	80	1	1	0.1	0.1
max.	70	125	90	20	25	3.0	3.0
Anti-reflective metasurface							
	p	h_{lower}	h_{upper}	w_{bottom}	w_{middle}	w_{top}	
min.	150	25	25	50	50	10	
max.	300	300	300	290	250	250	

When the gradient of the objective function is known, we consider the L-BFGS-B algorithm [19]. This method moves at each step in the direction of the steepest descent. In order to determine the step size, the method constructs a low-memory approximation of the inverse of the Hessian matrix of second partial derivatives.

Both local optimization methods are implemented based on the python package `scipy.optimize` [36].

A.2 Stochastic global optimization

As stochastic global optimization methods, we consider particle swarm optimization and differential evolution.

Particle swarm optimization has a simple algorithm. Each particle holds the information of the position $\mathbf{p} \in \mathcal{X} \subset \mathbb{R}^D$ of the lowest function value seen so far by the particle, and the position $\mathbf{s} \in \mathcal{X}$ of the lowest function value seen by the swarm. At each step random numbers r_d and q_d are chosen uniformly from $[0, 1]$ for each direction $1 \leq d \leq D$ and each particle independently. The velocity v_d of a particle in direction d is updated according to

$$v_d \leftarrow \omega v_d + \varphi_p r_d (p - x_d) + \varphi_s q_d (s_d - x_d),$$

where x_d is the current position of the particle in direction d . That is, the updated velocity is a weighted sum of the previous velocity, a velocity in direction of \mathbf{p} , and in direction of \mathbf{s} . The position of particle in direction d is updated according to $x_d \leftarrow x_d + v_d$.

Our implementation is based on the Python package `pyswarm` [37], which supports a parallel evaluation of the objective function. We extend the algorithm by initializing the particles by a Sobol sequence, excluding parameter values that do not meet the constraints. Furthermore, the random velocity and position update is repeated until the position meets all constraints. If this fails 100 times, the particle is randomly placed somewhere else in the constrained parameter space $\mathcal{X} \subset \mathbb{R}^D$. For the benchmark, we use the standard configuration of `pyswarm`, i.e. the weights ω , φ_p , φ_s are set to 0.5 and the swarm consists of 100 particles.

Differential evolution is a population-based genetic algorithm. The next generation is computed by creating new offsprings \mathbf{y} for each individual \mathbf{x} in the population by a weighted average (crossover) of some individuals $\mathbf{a}, \mathbf{b}, \mathbf{c} \in \mathcal{X}$ of the current generation. According to a fixed *crossover probability* (also termed *recombination constant*), random parameter dimensions $0 \leq i \leq D$ are selected. For these dimension, the parameter value of the offspring is set to $\mathbf{y}_i = \mathbf{a}_i + F(\mathbf{b} - \mathbf{c}_i)$, where F is called *differential weight* or *mutation constant*. If the offspring is fitter than its parent (i.e. it has a lower objective function value), it replaces the parent in the next generation. Differential evolution is implemented based on the python package `scipy.optimize.differential_evolution` [36, 38]. We use the standard parameters of the optimizer, i.e. `strategy='best1bin'`, `mutation=(0.5, 1)` and `recombination=0.7`. Moreover, we use a population size of 100 individuals. As in the case of particle swarm optimization, the algorithm is extended by initializing the individuals by a Sobol sequence meeting the constraints and by repeating the crossover until the offspring fulfills the constraints. Furthermore, we implemented a thread-based parallel evaluation of the fitness function.

A.3 Bayesian optimization

Bayesian optimization is based on a stochastic model of the objective function. Here, we use a Gaussian process (GP). Given previous observation of the objective functions, a GP can predict the function value and its statistical uncertainty for each point of the parameter space $\mathbf{x} \in \mathcal{X}$ by means of Gaussian process regression [30]. The accuracy of the prediction can be enhanced by incorporating derivative information on the objective function [40]. If available, we use this information in order to speed up the optimization process [46].

Based on this statistical information one can determine the expected improvement $\text{EI}(\mathbf{x}) = \mathbb{E}[\max(0, f_{\min} - f(\mathbf{x}))]$, i.e. the probabilistic expectation value of the one-sided difference $\max(0, f_{\min} - f(\mathbf{x}))$ between the function value $f(\mathbf{x})$ and the currently known lowest function value f_{\min} . The next sampling point is chosen at a position of large expected improvement.

In order to parallelize Bayesian optimization, we follow a proposal by González *et al.* [39]. Through a penal-

ization function $\phi(\mathbf{x})$, regions close to the parameter values of running calculations are avoided. That is, the next sampling point is chosen at a point of maximal penalized expected improvement

$$\mathbf{x}^* = \arg \max_{\mathbf{x} \in \mathcal{X}} [\phi(\mathbf{x})\text{EI}(\mathbf{x})].$$

The search for \mathbf{x}^* is performed with the L-BFGS-B method starting from a number N_{init} of different initial points drawn from a Sobol sequence. As described in the main text, this search process is adapted to balance the effort to find \mathbf{x}^* with the effort to compute the objective function.

More details on the Bayesian optimization approach can be found in [47, 48].

B Optimization strategies

The optimization strategies of the different methods are visualized in Fig. 5. For all optimization strategies the achieved coupling efficiencies are plotted as a function of one geometry parameter and as a function of the optimization progress. The figure shows, for example, that Bayesian optimization alternates between phases of exploitation (convergence into a found local minimum) and exploration (sampling away from all known local minima). Figure 5 reveals that the objective function has a large number of local minima since each parallel run of the downhill simplex algorithm converges to a different minimum.

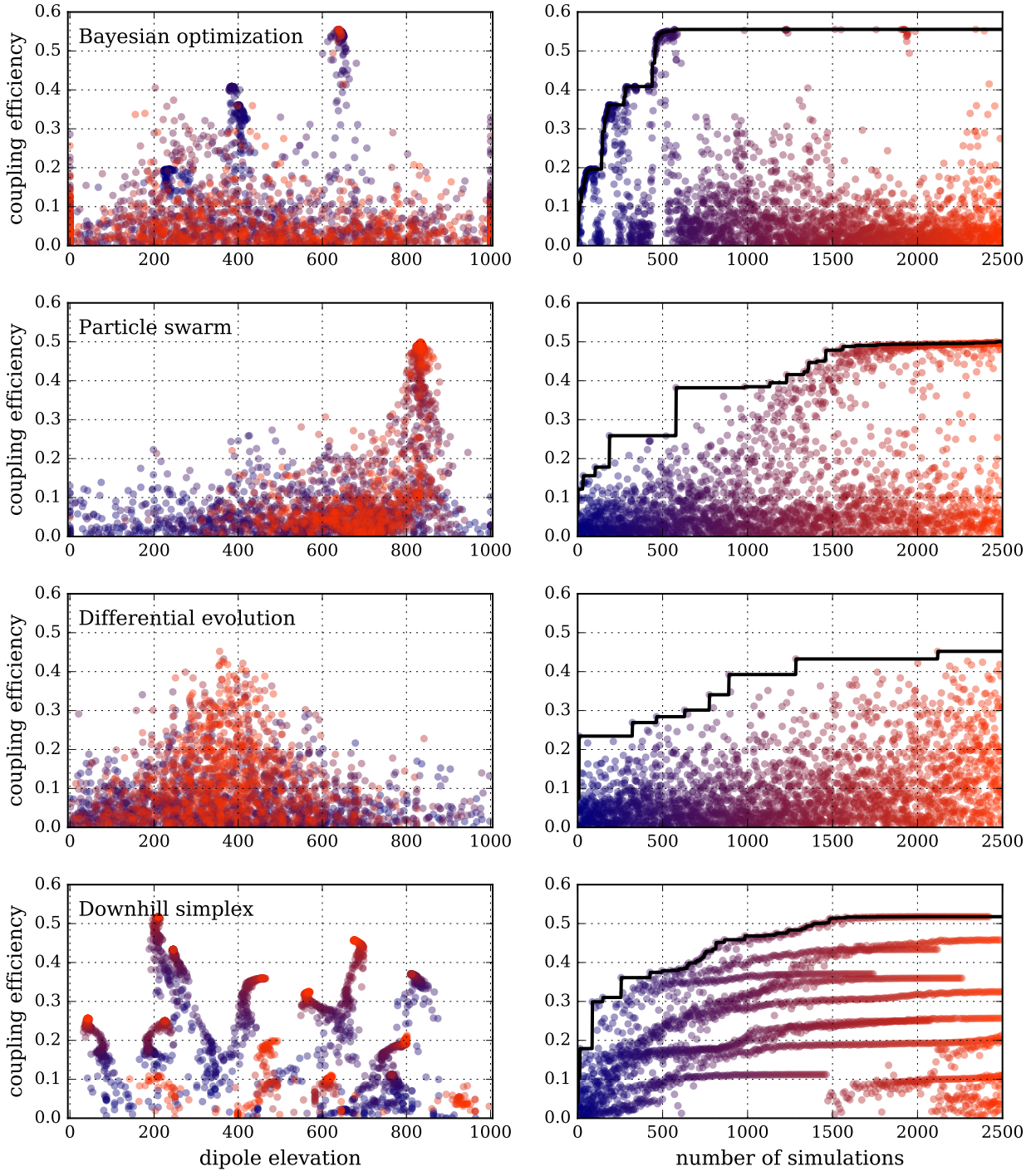


Fig. 5. **Left column:** Objective function value plotted against dipole elevation h_{dip} of the single-photon source for all samples drawn during a run of the different optimization approaches. **Right column:** Best seen objective function value plotted against the number of simulations for the same optimization run. The points are colored according to the number of simulation (dark blue at the beginning, light red at the end of the optimization). The graphs visualize the different strategies of the optimization approaches. **Bayesian optimization** probes sequentially different local minima. Whenever the expected improvement within a local minimum gets small, other parts of the parameter space are sampled until a better minimum is found (exploration). If this fails, the best found minimum is probed again (exploitation). **Particle swarm optimization** first probes the parameter space randomly. After about 500 simulations a good sample with close to 40% coupling efficiency is found. A part of the swarm moves into the direction of this swarm minimum. **Differential evolution** build new population members by changing some parameter values of existing members (point mutation). This leads to the formation of vertical lines on the left side (i.e. different individuals with the same dipole elevation). **Downhill simplex optimization** performs parallel local optimizations starting from different initial points. Each optimization run converges to a different local optimum. After convergence, the local optimization is restarted from a new position.